Available online at www.sciencedirect.com
SCIENCE DIRECT®
Nuclear Instruments and Methods in Physics Research A 550 (2005) 185–200
NUCLEAR INSTRUMENTS & METHODS IN PHYSICS RESEARCH Section A
www.elsevier.com/locate/nima

Separation of scintillation and Cherenkov light in an optical calorimeter

N. Akchurin[a], O. Atramentov[b], K. Carrell[a], K.Z. Gümüş[a], J. Hauptman[b], H. Kim[a], H.P. Paar[c], A. Penzo[d], R. Wigmans[a,*]

[a]*Texas Tech University, Lubbock, USA*
[b]*Iowa State University, Ames, USA*
[c]*University of California at San Diego, La Jolla, USA*
[d]*INFN Trieste, Italy*

Received 15 March 2005; accepted 31 March 2005
Available online 26 July 2005

Abstract

Simultaneous measurement of the scintillation and the Cherenkov light produced in hadronic shower development makes it possible to eliminate the effects of fluctuations in the electromagnetic shower fraction, which dominate and spoil the performance of non-compensating calorimeters. In this paper, we report on a study to separate the light signal produced by an optical calorimeter into its scintillation and Cherenkov components. To this effect, we use differences in the time structure of these two signals, as well as differences in the angular distribution of these two types of light. Both methods give useful results, especially when the numbers of scintillation and Cherenkov photons are comparable.

PACS: 29.40.Ka; 29.40.Mc; 29.40.Vj

Keywords: Calorimetry; Scintillation light; Cherenkov light; Optical fibers

1. Introduction

In a previous paper, we have demonstrated the beneficial effects of simultaneous measurements of the scintillation and the Cherenkov light produced in hadronic shower development [1]. In the development of showers initiated by hadrons and jets, Cherenkov light is only produced by the relativistic charged shower particles. Since the latter are predominantly produced in the electromagnetic (em) shower components of hadrons or jets, a comparison of the Cherenkov signal with

*Corresponding author. Tel.: +1 806 742 3779; fax: +1 806 742 1182.
E-mail address: wigmans@ttu.edu (R. Wigmans).

0168-9002/$ - see front matter © 2005 Elsevier B.V. All rights reserved.
doi:10.1016/j.nima.2005.03.175

the scintillator signal, to which *all* charged shower particles contribute, makes it possible to measure the energy fraction carried by the em component, f_{em}, event by event. As a result, the effects of fluctuations in this component, which are responsible for all traditional problems in non-compensating calorimeters (non-linearity, poor energy resolution, non-Gaussian response function), can be eliminated. This leads to an important improvement in the hadronic calorimeter performance.

These results make it not only possible to design excellent calorimeter systems for future experiments, for example at the proposed Linear Collider (ILC), but they also point the way to improving the hadronic performance of *existing* calorimeters. Especially experiments that use crystals to measure the energy carried by electrons and photons tend to have a rather poor performance for jets and hadrons, because of the large e/h ratio of these homogeneous calorimeters [2]. If, however, one were able to separate the light produced by these crystals into its scintillation and Cherenkov components, then the techniques from Ref. [1] could be used to improve the hadronic performance of such detectors too.

The study described in the present paper was carried out to investigate possible techniques to separate the two types of light from a medium that generates both. It focuses on techniques that exploit differences in the time structure of these two signals, and differences in the angular distribution of the two types of light. Other features in which the two signals differ concern the optical spectra and the polarization. However, the latter characteristics do not (yet) lend themselves easily to a practical method for separating the light produced by a calorimeter into its two components. In order to judge the effectiveness of the used techniques, it is of course crucial to know, event by event, how many photons of each type were produced. The detector used for these studies was uniquely suited to provide that information.

In Sections 2 and 3, we describe this calorimeter and the experimental setup in which it was tested. In Section 4, we discuss the experimental data and the techniques used to separate the scintillator and Cherenkov signals produced by the calorimeter. Experimental results are presented in Section 5 and conclusions are given in Section 6.

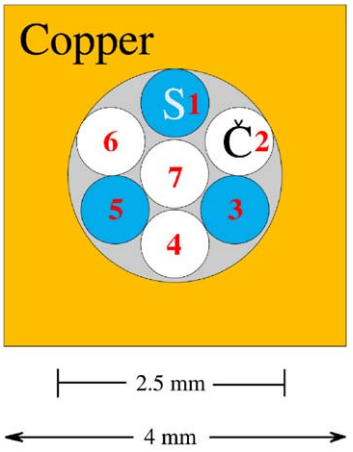

Fig. 1. The basic building block of the DREAM detector is a $4 \times 4\,mm^2$ extruded hollow copper rod of 2 m length, with a 2.5 mm diameter central hole. Seven optical fibers (4 undoped and 3 scintillating fibers) with a diameter of 0.8 mm are inserted in this hole.

2. The DREAM detector

The measurements described in this paper were performed with a calorimeter that has become known by its acronym DREAM, for Dual-REAdout Module. This detector is based on a copper absorber structure, equipped with two types of optical fibers, which measure the scintillation and the Cherenkov light produced by the shower particles.

The basic element of this detector (see Fig. 1) is an extruded copper rod, 2 m long and $4 \times 4\,mm^2$ in cross-section. This rod is hollow, the central cylinder has a diameter of 2.5 mm. In this hole are inserted seven optical fibers. Three of these are plastic scintillating fibers,[1] the other four fibers are undoped fibers, intended for detecting Cherenkov light. We used two types of fibers for the latter

[1]SCSF-81J, produced by Kuraray Co. Ltd, Tokyo, Japan.

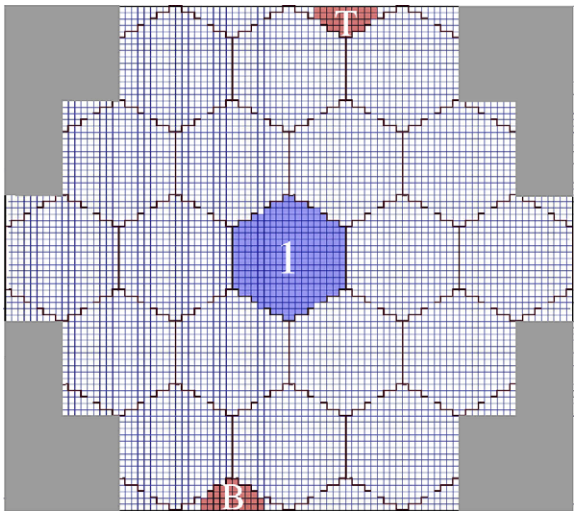

Fig. 2. Schematic layout of the DREAM calorimeter (front view). Each square represents a copper tube, shown in detail in Fig. 1. The subdivision into hexagonal readout towers is shown, and the areas used for the study described in this paper are marked by 1, T and B.

purpose. For the central region of the detector, high-purity quartz fibers[2] were used, while the peripheral regions of the detector were equipped with acrylic plastic fibers.[3]

The DREAM detector consists of 5580 such rods. The fibers were grouped to form 19 towers. Each tower consists of 270 rods and has an approximately hexagonal shape. The towers are longitudinally unsegmented. The readout structure is shown schematically in Fig. 2. The fibers sticking out at the rear end of this structure were separated into 38 bunches: One bunch of scintillating fibers and one bunch of Cherenkov fibers for each of the 19 hexagonal towers. In this way, the readout structure was established. Each bunch was coupled through a 2 mm air gap to a photomultiplier tube (PMT).[4] Many more details about this calorimeter and its performance characteristics are given in Refs. [1,3–5]. One performance characteristic that turned out to be particularly important for the present studies concerns the light yield of the Cherenkov fibers. This light yield was measured with 40 GeV em showers. It was found to be 8 photoelectrons (p.e.) per GeV for the towers equipped with quartz fibers, and 18 p.e./GeV for those equipped with plastic Cherenkov fibers [3].

For the purpose of the studies described in this paper, we equipped in addition the rods in the areas indicated with T (top) and B (bottom), which were initially only intended as fillers, with fibers. Each of these areas measured 5.8 cm^2. Each fiber was used in two rods, one rod in the T area and the corresponding (mirror image) rod in the B area. These fibers were about 6 m long, and were bent over 180° upstream of the calorimeter. In this way, both extremities of these fibers ended up in the readout area located at the downstream end of the calorimeter.

The fibers from the T and B areas were split into 3 bunches. One bunch contained 2 scintillating fibers from each rod, namely the fibers numbered 3 and 5 in Fig. 1. A second bunch contained 2 (plastic) Cherenkov fibers from each rod, numbers 2 and 6 (Fig. 1). The third bunch contained the remaining fibers (1 scintillating and 2 Cherenkov fibers from each rod, numbers 1, 4 and 7).

This splitting was done in the same way for the T and B areas, so that a bunch from the T area contained exactly the same fibers as the corresponding bunch from the B area. Each of these 6 bunches was coupled to a PMT in the same way as the 38 other bunches. These 6 PMTs were thus detecting light from both sides of the 3 fiber bunches.

The reason for this 3-way splitting was the following. The bunches containing only one type of fiber provided for each event the relative strengths of the scintillator and Cherenkov signals. The third bunch produced a signal from a mixture of these two types of light. The separation of this mixture into its components could thus be verified, event by event, by this arrangement. By reading out the same fibers from both ends, it became possible to study forward/backward asymmetries in the light production,

[2]Polymer-clad fused silica fibers, produced by Polymicro, Phoenix, Arizona, USA.

[3]Raytela PJR-FB750, produced by Toray, Japan.

[4]Hamamatsu R-580, 10-stage, 1.5-in. diameter.

which were expected to be quite different for the two types of light.

The PMTs reading out the scintillating fibers were equipped with a yellow filter[5] between the fiber ends and the photocathode. This filter increased the attenuation length (λ_{att}) of the scintillating fibers and reduced the overall scintillation light level to the point where the PMTs could accommodate both types of fibers. The same filters were also used for the scintillating fibers in the mixed bunches from the T and B areas. The latter fibers were for some of the measurements in addition equipped with neutral-density filters, which reduced the number of scintillating photons with a factor of 4, and changed the mixture of the two types of light in these bunches accordingly. Equipped with these filters, the attenuation length of the scintillating fibers was measured to be 5 m. For the plastic Cherenkov fibers, we found $\lambda_{att} = 8$ m.

3. Experimental setup

3.1. The beam line

The measurements described in this paper were performed in the H4 beam line of the Super Proton Synchrotron at CERN. The DREAM calorimeter was mounted on a platform that could move vertically and sideways with respect to the beam. The detector was oriented in such a way that the fibers were running parallel to the beam trajectory, i.e. the angles θ and ϕ between the fibers and the incident particles in the vertical and horizontal planes were both 0°.

We used several auxiliary detectors in these beam tests. These detectors served to obtain clean samples of the desired type of events and to measure the impact point of the particles in the calorimeter event by event.

Two small scintillation counters provided the signals that were used to trigger the data acquisition system. These Trigger Counters were 2.5 mm thick, and the area of overlap was $6 \times 6\,\mathrm{cm}^2$. A coincidence between the logic signals from these counters provided the trigger.

The impact point of the beam particles in the DREAM calorimeter was measured with a *fiber hodoscope*, which was installed about 3 m upstream of the front face of the calorimeter. This hodoscope consisted of ribbons of scintillating fibers oriented in the horizontal or vertical direction, thus providing the y and x coordinates of the beam particles. Details about this hodoscope, and examples of its excellent performance, are given in [3].

It was important to generate calorimeter signals that consisted of a mixture of Cherenkov and scintillation light that varied substantially from one event to the next. This was achieved by means of interaction products of nuclear reactions in an upstream target. For this purpose, a 10 cm thick polyethylene target ($\sim 0.1\lambda_{int}$) was installed in front of the calorimeter. Scintillation counters placed upstream and downstream of this target made it possible to recognize and select the desired events. Nuclear interactions of beam pions in the target could be selected, by requiring a mip signal in the upstream detector (indicating the passage of a single pion) and a much larger signal in the downstream counter. The latter signal could also be used as a measure for the multiplicity of the nuclear reactions.

For the measurements of beam electrons, this setup was replaced by a *preshower detector*, consisting of a 5 mm thick lead plate followed by a scintillation counter. This device was an efficient tool to remove contaminating pions and muons from the electron beam [3].

3.2. Data acquisition

The various detector signals were transported through RG-58 cables with (for timing purposes) appropriate lengths to the counting room. All signals, except those from the trigger counters and the fiber hodoscope, were digitized by 11-bit Lecroy 2249 W charge-sensitive ADCs. These had a gain of 4 counts/pC. The ADC gate width was 120 ns, safely long enough to capture the signals in their entirety. [We show in Section 5.1 that the scintillator signals had decreased to less

[5] Kodak, Wratten #3, nominal transmission 7% at 425 nm, 90% at 550 nm.

than 4% of their amplitude after 50 ns and that the Cherenkov signals were even smaller than that.]

The signals from the fiber hodoscope were digitized by TDCs. Eight TDCs were used, four for the horizontal and four for the vertical fiber ribbons, respectively. The time information was converted into the (x, y) coordinates of location of the point where the beam particle traversed the hodoscope.

The data acquisition system was based on CAMAC, interfaced via a VME bus to a Linux-based computer. A maximum of 2000 events were recorded in the 2.6 s SPS spill. The typical event size was ~150 bytes. All calorimeter signals and the signals from the auxiliary detectors were monitored on-line.

3.3. Calibration of the detectors

Using the high voltage, the gain in all PMTs was set to generate ~2 pC/GeV. The 38 PMTs reading out the 19 towers, as well as the 6 PMTs reading out the T and B areas, were calibrated with 40 GeV electrons. The showers generated by these particles were not completely contained. The (average) containment was found from EGS4 Monte Carlo simulations to be ~93% for the hexagonal towers and ~70% for the T and B areas. These factors were taken into account in determining the calibration constants.

4. Experimental data and methods

4.1. Methods to separate Cherenkov light from scintillation light

The fluorescent light produced in molecular de-excitation processes (scintillation light) differs in a number of characteristic ways from that generated by charged particles traveling faster than the speed of light (c/n) in a detector medium with an index of refraction n (Cherenkov light):

(1) The *time structure* of the signals is different. The generation of Cherenkov light is an instantaneous process. On the other hand, the emission of scintillation light is characterized by one or several time constants, which are typical for the molecular de-excitation processes that are taking place. In practice, other factors also contribute to the time structure of the calorimeter signals, in particular dispersion in the transit time of the PMTs and the difference between the speed of light in the fibers and the speed of the particles that generate the signals. However, for a given shower, the fraction of the Cherenkov light that is collected in a time interval (Δt) starting with the arrival of the first photons at the photocathode is larger than the fraction of the scintillation light collected in the same time interval. This difference also appears in the charge signals generated by this light. In this paper, we explore this feature by measuring the fraction of the calorimeter signal recorded in the "tail" of the shower, i.e. *beyond* Δt.

(2) The *angular distributions* of the light generated by both mechanisms are different. Scintillation light is emitted isotropically, the excited molecules have no memory of the direction of the particle that excited them. On the other hand, Cherenkov light is emitted at a characteristic angle by the shower particles that generate it. This Cherenkov angle, $\theta_C = \arccos(n\beta)^{-1}$, amounts in acrylic plastic to ~48°, for particles with $\beta \approx 1$. The relativistic shower particles have a non-isotropic angular distribution, with a preference for the direction of the incident particle that initiated the shower. As a result, the response of a fiber calorimeter that uses Cherenkov light as the source of its signals depends on the angle of incidence (θ) of the particles. This has been measured by several groups for electromagnetic showers [3,6]. As expected, the response reaches a maximum for θ close to θ_C. For angles of incidence $\theta \sim 0$, the response is lower by a factor of ≈ 2 and for angles $\theta \sim 90^\circ$ by a factor of ≈ 5. For angles $\theta > 90^\circ$, the response decreases further.
The signals observed for beam particles entering the calorimeter at an angle that falls outside the acceptance cone, defined by the numerical

aperture of the fibers,[6] are predominantly caused by relativistic shower electrons produced in Compton scattering [7]. For parallel incidence ($\theta = 0$), signals observed at the *upstream* end of the Cherenkov fibers are caused by relativistic Compton electrons traveling at angles around 132° (i.e., $180^\circ - \theta_C$) with the beam direction, while the signals observed at the *downstream* end are caused by relativistic shower electrons traveling at angles around ~48° (θ_C) with the beam direction. Since the angular distribution of these relativistic shower electrons strongly favors the latter ones, the backward/forward ratio was expected to be small (0.1–0.2) for the Cherenkov signals. For this reason, we believed a measurement of the ratio between the light emitted in the backward and forward directions to be a good tool for distinguishing scintillation and Cherenkov light. Reading out both ends of the optical fibers in which the calorimeter signals were generated provided the means to do this.

(3) The *optical spectra* of the light generated by both mechanisms are different. The Cherenkov light exhibits a characteristic λ^{-2} spectrum, while scintillation spectra are very crystal-specific and typically concentrated in a rather narrow wavelength range.

(4) Unlike scintillation light, Cherenkov light is *polarized*. Because of the directionality of the Cherenkov light, and because of the preferential direction of the shower particles emitting Cherenkov light (in the early shower component), this polarization is also expected to be observable in the calorimeter signals generated by em showers.

The latter two phenomena may be demonstrated by means of filters, which would have a different effect on the two types of light. In the studies described in this paper, we concentrated on (1) and (2).

[6]For the plastic Cherenkov fibers used in this calorimeter (numerical aperture 0.50), this acceptance cone covers angles of incidence $\theta = 48^\circ \pm 30^\circ$.

4.2. Experimental data

Events were triggered by coincident signals in the scintillation counters upstream of the calorimeter. Only events for which the (x, y) coordinates of the beam particle in the fiber hodoscope were measured were retained for the analyses described in this paper.

The following data sets were used for these analyses:

(1) Electron data at 80 GeV, in which the beam was sent into the center of the areas *T* and *B*. Because of the limited size of the *T* and *B* areas, the impact points of the beam particles were limited to a $3 \times 3\,\mathrm{mm}^2$ region in this analysis.

(2) Multiparticle events produced by interactions of 150 GeV π^+ in the polyethylene target. The pion beam was moved in six steps of 1 cm from the center of the *T* region to a point located 6 cm lower. Some data were also taken in the *T* center with 300 GeV π^+. In each run, 100 K events were collected.

(3) Electron data at 80 GeV, in which the beam was sent into the center of the calorimeter (Tower 1). The signals from the 2 PMTs viewing this tower were split into two parts, one of which was delayed with respect to the other. The delay time, Δt, was varied from 1 to 52 ns.

(4) Multiparticle events produced by interactions of 100 GeV π^+ in the polyethylene target. The pion beam was steered to the center of Tower 1 for these measurements. As in data set 3, the signals from this tower were split into 2 parts, one of which was delayed with respect to the other. The delay time was varied between 1 and 60 ns.

(5) A high-statistics data set of type 4, with $\Delta t = 12$ ns. About 2 million events were collected.

The measurements from data sets 1 and 2 were carried out twice, with and without the neutral-density filters that reduced the number of scintillation photons in the mixed signals by a factor of 4.

5. Experimental results

5.1. Measurements using the time structure of the signals

In this subsection, we describe our exploration of the fact that, for a given shower, the fraction of the Cherenkov light produced in a given time interval is different from the fraction of the scintillation light produced in that same interval. The experimental results are based on data sets 3, 4 and 5, and concern signals from the central calorimeter tower.

The PMT signals from this tower were split at the base into two equal parts. These signals were digitized by separate ADC's. One ADC (ADC1) was timed such that the start of the gate corresponded to the start of the signal (i.e., the arrival time of the first electrons that constituted this signal). The start of the gate of the other ADC (ADC2) was delayed by a time Δt with respect to the first one. By subtracting the digitized ADC2 signals from the ADC1 ones, it was thus possible to determine the fraction of the total signal that was recorded in the first Δt seconds after the start of the signal.

Fig. 3 shows results of this procedure, separately for the Cherenkov and the scintillator signals generated by 80 GeV electrons showering in this tower. The Cherenkov signals were indeed faster: In 10 ns, 53% of the total Cherenkov signal was recorded, versus 39% of the scintillator signal. After 20 ns, the fractions were 75% and 63%, respectively.

From the measured increments in these fractions, the average time structure of the two types of signals could be inferred. The result is shown in Fig. 4 (note the logarithmic vertical scale). The time structure is indeed distinctly different. Whereas the scintillator signal rises in a few nanoseconds to its maximum and then decreases exponentially with a time constant of ~14 ns, the time structure of the Cherenkov signal exhibits a narrow early peak (FWHM < 5 ns), followed by an exponential tail with approximately the same time constant as that of the scintillator signal. However, this tail seems to have some oscillation superimposed on it. The origin of the latter phenomenon is not understood.

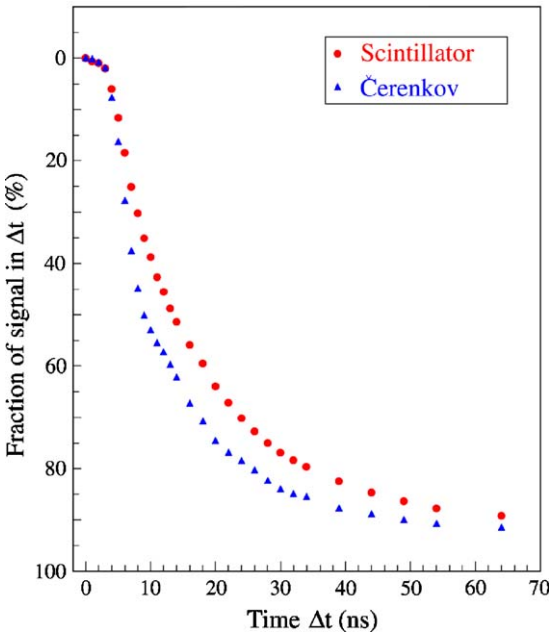

Fig. 3. Fraction of the total signal recorded in the first Δt seconds after the start of the signal, as a function of Δt. Results are given separately for the scintillator and Cherenkov signals from 80 GeV electron showers.

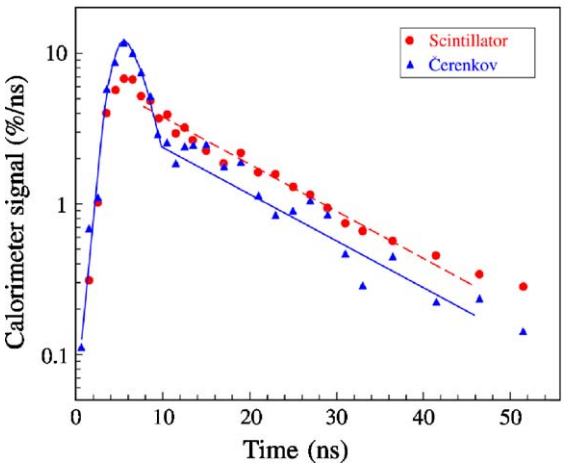

Fig. 4. The reconstructed (average) time structure of the Cherenkov and scintillator signals from 80 GeV electron showers in the DREAM calorimeter. The lines are drawn to guide the eye.

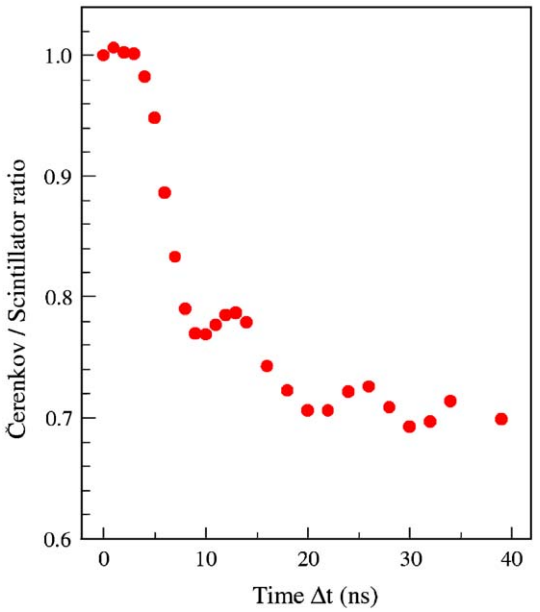

Fig. 5. Ratio of the average Cherenkov and scintillator signals from 80 GeV electron showers, digitized by ADC2. Only the fraction recorded beyond a time Δt after the start of the signals is thus taken into account. Results are given as a function of Δt.

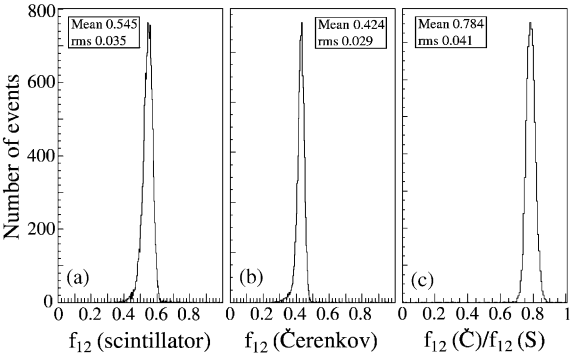

Fig. 6. Distribution of the fraction of the signals from 80 GeV electron showers recorded more than 12 ns after the start of the signal. Results are given for the scintillator (a) and Cherenkov (b) signals, and also for the ratio of both signals (c).

The observed differences provided a tool to discriminate between the two types of light and thus unravel a mixed signal into its components. Either the early or the late part of the observed signals could be used for this purpose. In order to maximize the sensitivity, the time cut should be made such that the selected part represents typically about half of the total signal.

We used the late part, or "tail", of the calorimeter signals, for this purpose. The ratio of the average signals from ADC2 and ADC1 corresponds to the average fraction of the signal that was recorded *after* the first Δt nanoseconds had passed. In the following, we refer to this fraction as $f_{\Delta t}$. Fig. 5 shows the average ratio of the Cherenkov and the scintillator ADC2 signals, as a function of the time Δt, for 80 GeV electron showers. The oscillations observed in the tail of the Cherenkov signals propagate into this distribution as well, but the overall tendency shows this ratio decreasing with time, leveling off after $\Delta t = 20$ ns. However, as Δt increased, the ADC2 signals also became rapidly smaller (see Fig. 3). As a result, the event-to-event spread in the ratio increased. There was thus an optimal Δt value, where the average ratio of the ADC2 signals was substantially different from 1, with relatively small event-to-event fluctuations. We chose $\Delta t \sim 12$ ns for this purpose. Typically about half of the signal charge was collected in that time, with a difference of 20–25% between the average ADC2 signals from the two types of light.

Fig. 6 shows distributions of the fraction of the signal contained in the tail beyond 12 ns (f_{12}), for the Cherenkov and the scintillator signals from 80 GeV electron showers. On average, 42% of the Cherenkov signal and 55% of the scintillator signal was contained in that tail. Fig. 6c shows the distribution of the ratio of these two tail signals. Its average value, $R_{\check{C}S} = \langle f_{12}(\check{C})/f_{12}(S)\rangle$ is 0.78 and the distribution has a relative width (σ/mean) of $\sim$5%.

Next, we investigated if and to what extent this ratio reveals something about the ratio of Cherenkov and scintillation light produced in a random event. We used 100 GeV "jet" events (data set 5) for this purpose, because in such events a much larger variety of Cherenkov/scintillator signal ratios occurred than in electromagnetic showers. In extreme cases, the "jet" might consist exclusively of photons (from π^0 decays), in another extreme case, there would be no em shower components at all. In the first case, one would

expect the value of $R_{\check{C}S}$ to be the same as for em showers, in the second case, it would be zero.

In order to estimate the discriminating power that in practice may be derived from the time structure of the signals, we did the following. For each event, we added the scintillator and Cherenkov signals from Tower 1, and we determined the fraction f_{12} for this summed signal. This fraction was compared with the actually measured ratio of Cherenkov and scintillation light. The results, shown in Fig. 7, reveal a correlation between these two variables. This means that the fraction of the total signal recorded in the tail is indeed a measure for the ratio of the two types of light.

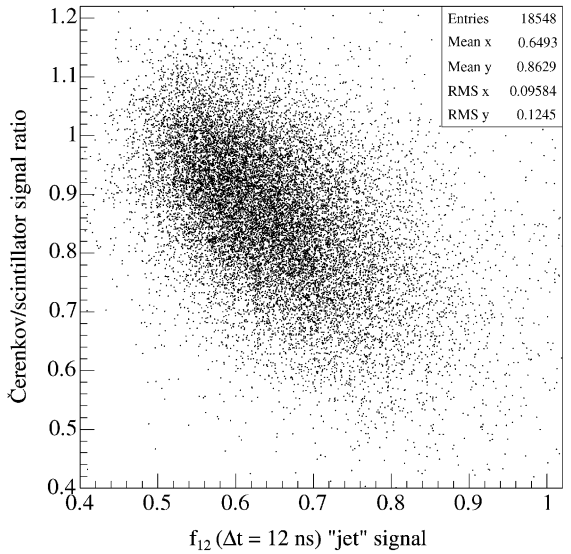

Fig. 7. The measured ratio of the Cherenkov and scintillator signals from 100 GeV "jets" versus f_{12}. This signal ratio is normalized to that for (80 GeV) electron showers.

More quantitative information about this correlation can be derived from Fig. 8. Fig. 8a shows the projection of the data points from Fig. 7 on the vertical axis, for a particular f_{12} bin, 0.60–0.61 in this case. The average ratio of the Cherenkov and scintillator signal components was 0.89. In Fig. 8b, the relationship between f_{12} and the average ratio of the Cherenkov and scintillator signal components is given for the entire range of measured values. The relative precision with which this ratio could be determined varied, event by event, from 10% to 15% (see Fig. 8a).

The event-to-event fluctuations were dominated by the effects of the low light yield in the (quartz) Cherenkov fibers (8 photoelectrons per GeV for em showers [3]). This can be seen as follows. For 80 GeV electron showers, the ADC1 and ADC2 signals consisted typically of 600 and 300 photoelectrons, respectively. Based on statistical fluctuations in these numbers, one should thus expect a fractional width of ~7% for the f_{12} distribution of

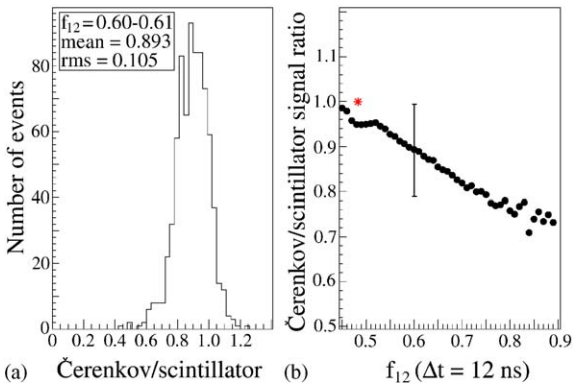

Fig. 8. The measured ratio of the Cherenkov and scintillator signals from 100 GeV "jets", for events in which 60–61% of the signal was recorded more than 12 ns after the start of the signal (a). The relationship between this signal ratio and the percentage of the signal recorded in the tail (b). The vertical bar indicates the event-to-event spread in this relationship, i.e. the rms width of distributions such as the one in Fig. 8a. The asterisk represents the result for 80 GeV electron showers.

these events, in good agreement with the experimental result (Fig. 6b). Because of the much larger side leakage, the signals from 100 GeV "jets" in Tower 1 were typically a factor of 2 smaller than those from 80 GeV electrons. The f_{12} fluctuations resulting from photoelectron statistics were thus correspondingly larger.

One clarification is needed at this point. The relationship depicted in Fig. 8b is, in first approximation, *not* dependent on the type or energy of the particle(s) that generated the signal, or the selected shower region. The relationship is solely based on the fact that the (charge) signals resulting from scintillation light generated in the detector have a different time structure than the signals resulting from Cherenkov light. In first approximation, it does not matter how these signals were generated. This may be illustrated by the fact that the relationship shown in Fig. 8b, which was derived from the signals generated by 100 GeV "jets" in a narrow hexagonal tower surrounding the jet axis, also describes the data point for 80 GeV electrons. However, as illustrated in the following, this first approximation is in some respects an oversimplification.

Further studies of the time structure of the signals from this calorimeter revealed several other interesting details. Fig. 9 shows the ADC1 and ADC2 scintillator signals from 80 GeV electron showers. Remarkably, the high-side tail that characterizes the total (ADC1) signal distribution is absent when we look at the signals from ADC2, i.e. the signals to which the charge collected in the first 12 ns did not contribute. The origin of this phenomenon can be understood from Fig. 10, which shows y distributions of the impact points of the particles generating the events. Fig. 10a depicts the y distribution for all events, whereas Fig. 10b shows the y distribution of the impact points for the events that produced a signal of more than 1400 ADC counts in Fig. 9a. Clearly, the latter event sample consists almost exclusively of events in which the beam particles entered the detector in one of the holes filled with fibers. It is well known that the calorimeter response, in the scintillator channel, is larger than average for such particles [3]. Since the radiation length of plastic amounts to ~40 cm, these particles developed showers much deeper inside the calorimeter than particles that entered in the copper absorber matrix. And since

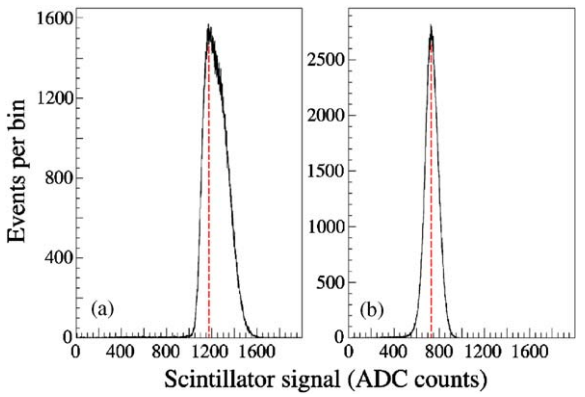

Fig. 9. Distributions of the measured scintillator signals from 80 GeV electron showers. Shown are the entire signals (a) and the portion recorded more than 12 ns after the start (b). The dashed lines represent the most probable signal values.

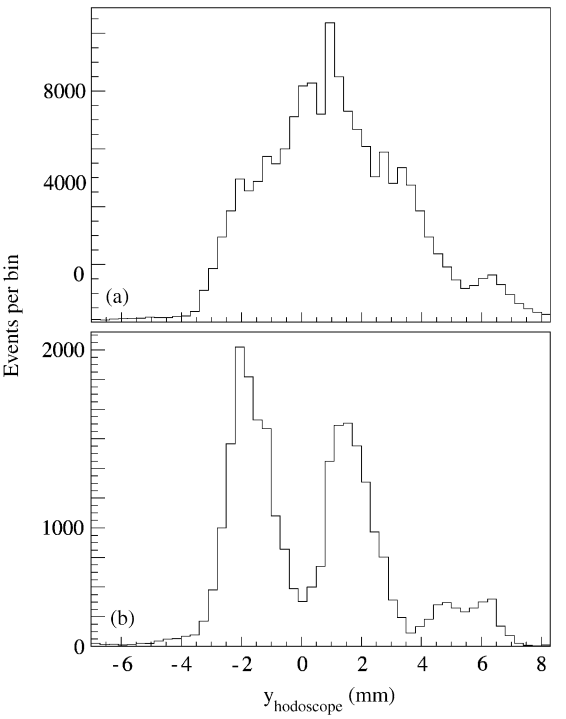

Fig. 10. Impact point distributions of events induced by 80 GeV electron showers. Shown are the y-distributions for all events (a) and for events from the high-side tail of the scintillator spectrum (more than 1400 ADC counts, (b)).

they traveled at a speed close to c, while the light produced in the fibers traveled at a speed c/n, their signals *started* 1–2 ns *earlier*. Therefore, the $\Delta t =$ 12 ns delay translated for these events into a delay that amounted to ~13–14 ns. As a result, a larger than average fraction of the signal was cut and the high-energy tail is more or less absent from the distribution in Fig. 9b.

As we showed and explained in previous papers [3,5], the broadening observed in Fig. 9a was absent for the Cherenkov signals. It also disappeared in the scintillator signals when the incoming electrons traveled at a small angle (a few degrees) with the fiber direction. Since this effect also broadened the distribution of the ratio of the Cherenkov and scintillator signals, one might wonder why this angle was chosen to be zero in these measurements. Because of the small instrumented (T,B) area, we wanted to minimize the effects of shower leakage on our calibration measurements. Also, a narrow distribution of the Cherenkov/scintillator signal ratio would not have served any essential purpose for the present studies. And only *because* we decided to choose for parallel incidence ($\theta = \phi =$ 0) did we observe the unexpected phenomena shown in Figs. 9 and 10.

5.2. Measurements using the directionality of the light

The second method we studied in light of its potential discriminating power between Cherenkov and scintillation light is based on differences in the directionality of these two different types of light. For reasons discussed in Section 4.1, the measured ratio of light emitted in the backward and forward directions was believed to be a good parameter for distinguishing scintillation and Cherenkov light. Our experimental setup was designed to study the discriminating power of this parameter. By reading out the fibers from both ends, the backward/forward ratio could be measured in a very direct way. For the scintillating fibers, the two signals should only be affected by the difference in the path length the light has to travel, typically ~1 m. Given the attenuation length of ~5 m, the effects of additional light attenuation in this 1 m reduced the backward signals to ~80% of the forward ones. However, because of the directionality of the Cherenkov light, the reduction of the backward Cherenkov signals was substantially larger than for the isotropic scintillator signals (see Section 4.1).

This is illustrated in Fig. 11, which shows separately the distributions of the backward/forward signal ratios for scintillation and Cherenkov light produced by 80 GeV electron showers in the Top area (data set 1). On average, the backward Cherenkov signals were a factor of 6 smaller than the forward ones from these showers, whereas the two scintillator signals differed only by ~20%.

The distribution of the mixed signals from these electron showers depends obviously on the relative contribution of both types of signals to the mix. The results shown in Fig. 12a were obtained with neutral density filters, which reduced the number of scintillating photons by a factor of 4. Without these filters, scintillating photons dominated the mixed signal, and the backward/forward ratio of these signals was only slightly different from that for pure scintillation light. However, with the filters a more or less balanced mixture between the two types of light was obtained.

The distributions from Figs. 11 and 12a are relatively narrow. This reflects the fact that all em showers are similar in these backward/forward characteristics. The width of these distributions is dominated by photoelectron statistics. For

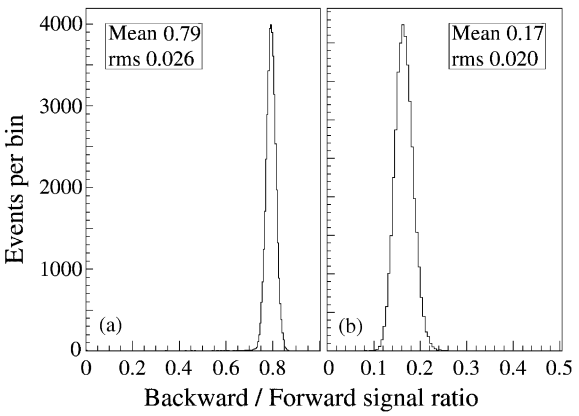

Fig. 11. The backward/forward ratio of the scintillator (a) and Cherenkov (b) signals generated by 80 GeV electron showers.

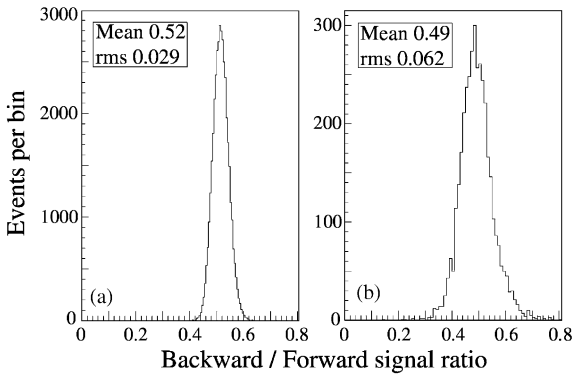

Fig. 12. The backward/forward ratio of the mixed Cherenkov/scintillator signals generated by 80 GeV electron showers (a) and 150 GeV "jets" (b).

example, the forward and backward Cherenkov signals from 80 GeV electron showers consisted typically of 500 and 90 photoelectrons, respectively.[7] Therefore, statistical fluctuations in these numbers led to a width (σ/mean) of ~12% for the distribution of the backward/forward Cherenkov signal ratio, in good agreement with the measured value (Fig. 11b). Because of the larger light yield in the scintillating fibers, the signal distributions shown in Figs. 11a and 12a are correspondingly narrower.

For the same reason as with the method discussed in the previous subsection, we studied the merits of this method with 150 GeV "jets" (data set 2). By selecting interactions in the upstream target with a multiplicity of at least 4, a variety of energy deposits and, more importantly, Cherenkov/scintillator signal ratios were generated. The pion beam generating these interactions was directed at the Bottom area for these studies. Fig. 12b shows the backward/forward ratio distribution measured for the mixed signal from these "jets". Because of the large lateral leakage, the average energy measured in the Bottom area for this event sample was only ~30 GeV. The variety in the Cherenkov/scintillator signal ratio for this event sample should manifest itself through the width of the distribution of the backward/forward ratio of the mixed signals. This width was indeed more than twice as large as for the electron showers. However, at least two other effects contributed to this broadening:

(1) Because of the smaller deposited energy, the numbers of photoelectrons constituting the signals were smaller. Therefore, the fluctuations in the number of photoelectrons were larger than for 80 GeV electron showers. These fluctuations were especially important in the backward Cherenkov signals.
(2) Longitudinal fluctuations in the deposited energy were considerably larger than for electron showers. These fluctuations had an effect on the width of the distribution of the backward/forward signal ratio, especially for the scintillator signals. Light attenuation in the fibers affected this ratio twice, because late (early) shower development both led to larger (smaller) signals in the forward direction *and* smaller (larger) signals in the backward direction. Because of the shorter light attenuation length, the scintillator signals were more affected by this than the Cherenkov signals.

Light production took place deeper inside the calorimeter than for electron showers, and the resulting increased light attenuation also affected the *average* backward/forward signal ratio for the scintillator signals. This ratio which, as we saw above, was for the isotropically emitted scintillation light completely determined by the effects of light attenuation, decreased from 0.79 for electron showers to 0.65 for the 150 GeV "jets". Since the backward/forward ratio for the Cherenkov light was completely dominated by the intrinsic directionality of this light (and *not* by light attenuation), the average values for electrons and jets were not very different, ~0.16 in both cases. As a result of this, also the distribution of the backward/forward ratio for the mixed (Cherenkov, scintillator) signals had a smaller average value for the jets than for the electrons (see Fig. 12), even though

[7]The light yield of the plastic Cherenkov fibers was measured to be 18 p.e./GeV, for the standard configuration of 4 such fibers per rod. The mixed-signal channels of the T, B areas contained only 2 Cherenkov fibers per rod, and the em showers were only 70% contained, so that the measured signals corresponded to 56 GeV.

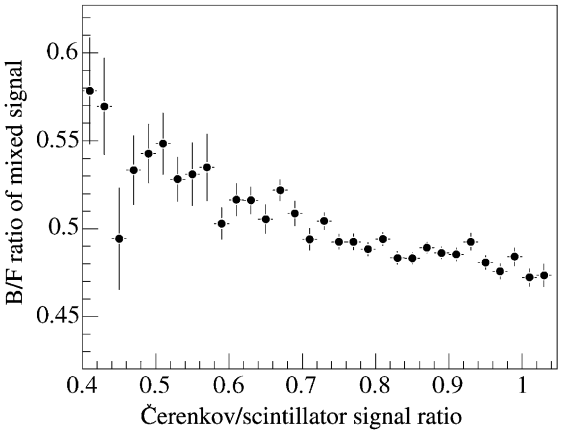

Fig. 13. The backward/forward ratio of the mixed Cherenkov/scintillator signals from 150 GeV "jets" as a function of the measured ratio of the "pure" Cherenkov and scintillator signals.

the relative contribution of scintillation light was larger for the jet signals.

As with the method discussed in the previous section, a numerical assessment of the discriminating value of the backward/forward ratio parameter requires an event-by-event analysis. Results of this analysis are shown in Fig. 13, which shows the relationship between the actually measured Cherenkov/scintillator signal ratio and the backward/forward ratio of the mixed signals. The correlation between these two parameters, although evident from the data, is not as good as one might like to see. There are two reasons for that:

(1) The small number of photoelectrons, especially in the backward Cherenkov signals, led to large fluctuations. These obscured the correlation.
(2) Because of the small detector area that was equipped for the forward/backward studies, and the need to have relatively large energy deposits (signals), we had to restrict the event sample to the central core region of the showers initiated by the jets. This limited the variety of Cherenkov/scintillator signal ratios in the event sample. Large differences between the two types of signals are mainly occurring in the peripheral shower regions, which are populated by particles which do produce scintillation light, but no Cherenkov light.

To circumvent the second problem, we used the same technique as for the method based on differences in the time structure of the two types of signal (Section 5.1). Rather than using the mixed signals from the triangular areas, we used the pure scintillator and quartz signals themselves to construct mixed signals. This made it possible to study the effects of varying the relative strengths of these two signal components.

As was shown in an earlier analysis [1], the ratio of the total Cherenkov and scintillator signals from hadronic showers in this detector (Q/S) is related to the electromagnetic shower fraction, f_{em}, as

$$\frac{Q}{S}=\frac{f_{\mathrm{em}}+0.21(1-f_{\mathrm{em}})}{f_{\mathrm{em}}+0.77(1-f_{\mathrm{em}})}. \tag{1}$$

Since f_{em} varies between 0 and 1, Q/S has in practice values between 0.3 and 1, the latter being the value for the electromagnetic showers used to calibrate the instrument. In the present study, where only the signals from one hexagonal tower were considered and shower tails were ignored, the range of possible Q/S values was further reduced. The event samples contained almost no events with $Q/S<0.5$.

In order to study the precision with which information on Q/S, and thus f_{em}, could be extracted from the forward/backward ratio of mixed calorimeter signals, we added the Cherenkov and scintillator signals, giving a relative weight α to the latter:

$$I=Q+\alpha S \tag{2}$$

and determined the backward/forward signal ratio distributions for these mixed signals, $B/F(I)$. These distributions were divided into 0.02 wide bins. Next, we made distributions of the Cherenkov/scintillator signal ratio for each of these bins. The mean value of the latter distributions is plotted as a function of $B/F(I)$.

Some results of this procedure are given in Fig. 14, for $\alpha=1$ (the full circles), $\alpha=5$ (the squares) and $\alpha=0.2$ (the triangles), respectively. For reference, the average backward/forward va-

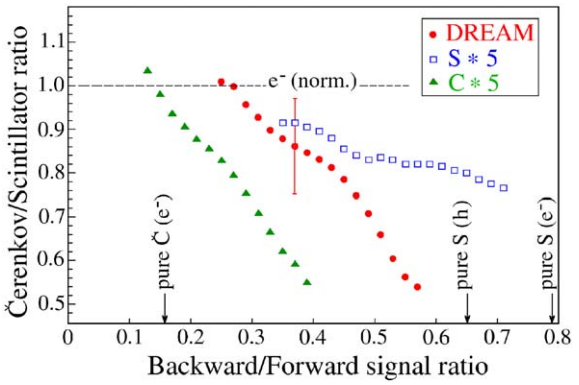

Fig. 14. The average ratio of the Cherenkov (Q) and scintillator (S) signals from 150 GeV "jets" in the DREAM calorimeter, as a function of the backward/forward ratio of mixed Cherenkov/scintillator signals. The latter were obtained as a weighted sum of the measured Cherenkov and scintillator signals: $I = Q + \alpha S$, with $\alpha = 1$ (the full circles), $\alpha = 5$ (the squares) and $\alpha = 0.2$ (the triangles), respectively.

lues for pure Cherenkov and scintillator signals are indicated as well in this figure. The vertical error bar gives a typical rms width of the distribution whose average value is plotted in the figure.

These data demonstrate the correlation between the average backward/forward ratio of these mixed signals and the relative contributions of Cherenkov and scintillation light to these signals. The correlation depends on the value of α. On average, the Cherenkov/scintillator ratio in these "jet" signals is about 0.8. For the unweighted DREAM data (i.e., for $\alpha = 1$), this corresponds to a backward/forward ratio of $\sim 0.4-0.5$. Events with a backward/forward ratio of 0.3 are indicative of an above-average Cherenkov component, i.e. a relative large em shower component, while events with a backward/forward ratio of 0.6 are likely to have a small em shower component.

When $\alpha = 5$, the correlation is clearly less strong. The figure shows that the most likely value of the Cherenkov/scintillator ratio is not far from the average value of 0.8, irrespective of the measured backward/forward signal ratio. Because of the reduced weight of the Cherenkov component in the total signal, the Q/S distributions of which the average values constitute the data in Fig. 14 are more determined by the tails of the response function for average events than by the very small backward/forward ratio of the Cherenkov contribution.

A similar insensitivity occurs when the signals are weighted in favor of the Cherenkov component (e.g., $\alpha = 0.2$). In that case, a relatively large value of the backward/forward ratio may as well be caused by the high-end tail of the response function for Cherenkov light as by a genuinely small contribution of Cherenkov light to the signal.

The sensitivity of the backward/forward method to the value of the em shower component can be expressed in terms of the weighting parameter α, for example as follows. The Q/S ratio for jets ranges from 0.28 (0.21/0.77, see Eq. (1)) to 1.0, and the backward/forward ratio varies between 0.165 for pure Cherenkov light to 0.647 for pure scintillation light. These ranges correspond to about a factor of 4 in both cases. The best sensitivity is thus obtained when a given change in the measured backward/forward signal ratio corresponds to the same fractional change in the Q/S value derived from this measurement. For example, if a 10% change in the measured value of B/F only leads to a 2% change in the predicted Q/S ratio, as for the $\alpha = 5$ case in Fig. 14, then the measured backward/forward ratio of the mixed signal is not a very sensitive parameter for determining the composition of the signal.

We therefore defined the sensitivity through a parameter ξ, which measures this relationship between the derivatives of Q/S and B/F. If a 10% change in B/F causes a 2% change in Q/S, then $\xi = 0.2$. The larger the value of ξ, the larger the precision with which the em shower fraction can be determined from the backward/forward ratio of the mixed signals. Fig. 15 shows how ξ varies with α. Maximum sensitivity, i.e. the best separability of the mixed signals into their Cherenkov and scintillation components, is reached for $\alpha \sim 0.5-1$, i.e. when the signals are slightly weighted in favor of the Cherenkov component. This is probably a consequence of the fact that the number of photoelectrons per unit of energy was smaller for the Cherenkov component than for the scintillation component, even after the latter signals were attenuated by means of

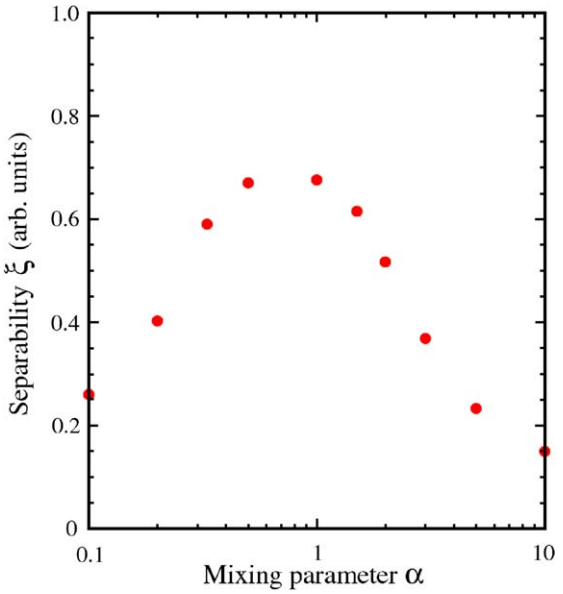

Fig. 15. Separability of the Cherenkov and scintillation components through the backward/forward ratio of mixed signals, as a function of the average relative contribution of both components to these signals. The larger the value of ξ, the better the signals can be separated into their components. See the text for details.

neutral-density filters. After this weighting, the numbers of photoelectrons, and thus the effects of statistical fluctuations, become comparable for the two components.

6. Conclusions

We have studied two techniques that make it possible to separate the light signals produced by an optical fiber calorimeter into their Cherenkov and scintillation components. These techniques are based on the different time structure of these signal components and on the different angular distribution of the two types of light. Both techniques produced useful results. In both cases, we observed a correlation between a measured property of the signals and the ratio of the numbers of Cherenkov and scintillation photons. This correlation, and thus the quality of the achievable separation, depended on the relative contributions of the two types of light to the calorimeter signals. Best results were obtained when these relative contributions were about the same. In both cases, the low light yield of the Cherenkov fibers was the dominating factor that limited the achievable separation.

We would like to emphasize that the techniques used to unravel the signals are by no means limited to fiber calorimeters. They can be applied in *any* calorimeter that produces optical signals, possibly with much better results than those reported here. The main reason for using a fiber calorimeter for these studies (apart from the fact that this instrument already existed) was that it allowed us to measure the relative strengths of the scintillator and Cherenkov signals independently, and thus verify the quality of the achieved separation in the mixed signals, event by event. However, a dedicated instrument could be designed such as to optimize the separability of the two types of signals, which was not a design consideration for the calorimeter used for our studies. Increasing the Cherenkov light yield would be an obvious first step.

Acknowledgements

We gratefully acknowledge the contributions of Tracy McAskill, Vladimir Nagaslaev, Alan Sill, Veronica Stelmakh, Yunyong Wang, Erika Washington and Kim Zinsmeyer to the construction of the DREAM detector. We thank CERN for making particle beams of excellent quality available. Our beam tests would not have been possible without the help we received from Claude Ferrari and Maurice Haguenauer. We thank K. Kuroda for loaning us the fiber hodoscopes. This study was carried out with financial support of the United States Department of Energy, under contract DE-FG02-95ER40938, and the Advanced Research Program of the State of Texas.

References

[1] N. Akchurin, et al., Nucl. Instr. and Meth. A 537 (2005) 537.
[2] R. Wigmans, Calorimetry—Energy Measurement in Particle Physics, International Series of Monographs on Physics, vol. 107, Oxford University Press, Oxford, 2000.

[3] N. Akchurin, et al., Nucl. Instr. and Meth. A 536 (2005) 29.
[4] N. Akchurin, et al., Nucl. Instr. and Meth. A 533 (2004) 305.
[5] N. Akchurin, et al., Comparison of high-energy electromagnetic shower profiles measured with scintillation and Cherenkov light, Nucl. Instr. and Meth., accepted, doi:10.1016/j.nima.2005.03.169.
[6] O. Ganel, R. Wigmans, Nucl. Instr. and Meth. A 365 (1995) 104.
[7] N. Akchurin, R. Wigmans, Rev. Sci. Instr. 74 (2003) 2955.